ISSN 1330-3651 (Print), ISSN 1848-6339 (Online)
Received: 11 November 2025; Accepted: 13 February 2026

https://doi.org/10.17559/TV-20260116003301
Original scientific paper

Adaptation of Agronomic Multispectral Cameras for Photodocumentation of Human Tissue During Thyroid Surgery

Dinka RADONIĆ*, Jana ŽILJAK GRŠIĆ, Ivan RAJKOVIĆ, Krešimir GRŠIĆ

Abstract: Multispectral imaging (MSI) enables the acquisition of visual information across multiple isolated visible and near-infrared spectral bands, thereby extending the capability of biological tissue differentiation beyond standard RGB recording. This paper investigates multispectral photodocumentation of a thyroid surgical procedure using two cameras, each providing three spectrally isolated channels. The study examines the feasibility of repurposing portable multispectral cameras originally designed for agronomic remote sensing for enhanced documentation of surgical procedures.
The required technical adaptations are described, and the information captured within individual spectral regions under intraoperative conditions is analyzed. Image acquisition was performed in a real operating room environment, and the recorded data was decomposed into individual spectral channels to examine information not visible to the unaided eye in both the visible and near-infrared ranges. The results confirm the feasibility and repeatability of the proposed approach and establish the fundamental steps for adapting such cameras for surgical photodocumentation. The findings demonstrate that existing, relatively affordable, and readily accessible equipment can be repurposed, and that the resulting multispectral material is suitable for integration into medical education.

Keywords: camera adaptation; camera repurposing; channel separation; medical education; multispectral imaging; surgical documentation

1 INTRODUCTION

Photographic and video recordings are increasingly used in scientific disciplines as auxiliary or primary research tools. Over the past two decades, the development of digital imaging in scientific applications has been characterised by several concurrent technological advancements. On one hand, improvements in technical image quality, including higher spatial resolution, increased dynamic range, and compression methods with minimal information loss, have contributed to an expanded information content of recorded data. On the other hand, imaging beyond the conventional RGB range has become feasible, enabling data acquisition in spectral regions that are invisible to the human eye but carry additional information about the recorded material.

Multispectral imaging (MSI) has been established in a wide range of application domains due to its ability to capture spectrally isolated information that extends beyond standard RGB representation. MSI records image data across multiple wavelengths and corresponding spectral signatures (endmembers) generated by reflection, absorption, or emission of radiation, depending on the material composition of the observed object [1]. In agronomy and forestry, multispectral cameras have been widely adopted to record vegetation reflectance in selected spectral bands. Based on these measurements, vegetation condition indices such as the Normalized Difference Vegetation Index (NDVI) are calculated, and plant species can be differentiated according to their spectral signatures [1]. By utilising isolated spectral bands, MSI improves the discrimination of different chromophores in tissue. As a result, it is currently applied in precision agriculture, cultural heritage conservation, environmental monitoring, and biochemistry [2-6].

In surgical practice, particularly in thyroid and parathyroid surgery, there is an additional requirement to preserve parathyroid tissue while ensuring its clear and reliable documentation during the operative procedure [7, 8]. In endocrine surgery, hyperspectral and multispectral analyses of glandular tissues performed during thyroid and parathyroid operations have demonstrated that different tissue types can be reliably distinguished based on their reflectance characteristics within a limited number of spectral bands [9]. Of particular relevance for intraoperative identification of the parathyroid glands is near-infrared (NIR) autofluorescence, where excitation using a light source at approximately 785 nm produces an emission peak in the range of 820-830 nm, enabling real-time identification of the glands without the administration of exogenous contrast agents [7]. Clinical studies and meta-analyses report high specificity and applicability of this method for the identification and preservation of parathyroid tissue [7, 8, 10, 11]. However, the majority of such systems have been developed as specialized medical equipment that is costly, limited in availability, and often restricted in long-term use due to circulation between hospitals and across national healthcare systems.

This paper presents an approach that does not assume the need to develop a new medical imaging device. Instead, it investigates whether an existing, readily available, portable multispectral camera originating from the agronomic domain, which incorporates three stable and spectrally isolated bands, can be employed in the operating room with appropriate optical adaptations. Although originally designed for agricultural applications, such cameras are repurposed for medical documentation due to their ability to provide information not accessible through standard photographic recordings at relatively low cost. The study examines the feasibility of multispectral imaging during thyroid surgery using unmodified surgical lighting conditions, without disrupting the surgical workflow and without the use of specialised medical optical equipment.

Medical studies upon which this work is based consistently report that the near-infrared (NIR) spectral region provides improved visualisation of glandular tissue and blood. Differences between the thyroid gland and surrounding anatomical structures are more pronounced in the NIR range than in standard RGB imaging, and this information can be utilised for more reliable tissue identification and preservation [7, 9, 11, 12]. Based on

these findings, it is expected that imaging using isolated visible spectral bands in combination with an NIR channel in the operating room will provide information that is not available in conventional RGB recordings. With respect to wavelength selection in MSI, previous measurements and studies indicate that shorter wavelengths emphasise surface contrast and vascular structures. Mid-range wavelengths support tissue differentiation due to the absorption characteristics of haemoglobin, while longer NIR wavelengths penetrate deeper into tissue and reveal information beyond the standard visible spectrum [9, 12- 15].

Unlike hyperspectral systems that employ a large number of contiguous spectral channels, multispectral imaging uses a limited set of carefully selected bands. This characteristic makes MSI more suitable for the dynamic conditions of an operating room due to faster acquisition, improved mobility, and a reduced equipment footprint [9, 12]. In medical applications, studies have shown that MSI in the visible and extended near-infrared (NIR) spectral ranges reveals subtle tissue differences that are not perceptible to the unaided eye, including successful applications in the dermatological assessment of skin lesions [5, 16-18]. These findings support the premise that multispectral recordings can complement existing visual information in the region of the thyroid gland and adjacent anatomical structures.

This paper presents a multispectral imaging technique aimed at differentiating information across spectrally isolated visible and near-infrared bands in the context of recording and analysing human tissues during a surgical procedure. The repurposing of cameras from the agronomic domain represents a logical step, as MAPIR Survey3N™ (OCN, NGB) camera models were originally developed for vegetation imaging and the detection of spectral differences beyond standard RGB recording [19, 20]. This capability to register information that is not visible to the unaided eye motivates the investigation of whether the same technology can be applied to human organic tissue in order to record spectral differences between anatomical structures that cannot be captured using conventional RGB documentation [19, 20].

The reproduction of recorded materials from surgical procedures also has educational relevance. In practice, the work of the lead surgeon can typically be observed by only a few students simultaneously, while the actual demand is considerably higher. Previous studies have highlighted challenges faced by students and residents observing surgical procedures, noting that key areas of the surgical field are often obscured from the observer's viewpoint [21]. For these reasons, 2D and 3D video recordings of surgical procedures have been developed and introduced [22-27]. The integration of a multispectral layer into this practice enables instructors to present the same surgical procedure in both the visible spectrum and the near-infraredrange, which is not perceptible to the human eye.

Video and photographic documentation in medical education has experienced substantial growth and has demonstrated statistically significant improvements when used as a complement to standard teaching methods, such as the flipped classroom approach, thereby addressing temporal and logistical constraints of clinical training [24-27]. Within this framework, multispectral documentation emerges as a means of increasing the informational content of recorded material, as well as the resulting educational value. The objective of this paper is to examine the feasibility and informational value of repurposing agronomic multispectral cameras for imaging thyroid surgery, and to evaluate the contribution of selected spectral bands to the differentiation of relevant anatomical structures, with particular emphasis on educational applications.

2 MATERIALS AND METHODS

Agronomic MSI cameras MAPIR Survey3N™ OCN (orange, cyan, NIR) and NGB (NIR, green, blue) were used in this study. These cameras were originally developed for vegetation imaging and the detection of spectral differences and provide fixed, spectrally isolated bands in the visible and near-infrared (NIR) ranges. Multispectral Camera 1 (MAPIR Survey3N/OCN) records spectrally isolated bands covering the visible orange region with a spectral peak at 615 nm, the cyan region with a spectral peak at 490 nm, and a near-infrared band with a spectral peak at 808 nm, which lies outside the visible spectrum. Multispectral Camera 2 (MAPIR Survey3N/NGB) is designed to record spectrally isolated bands comprising a near-infrared band with a spectral peak at 850 nm, outside the visible spectrum, as well as visible bands in the green region with a spectral peak at 550 nm and the blue region with a spectral peak at 475 nm.

The spectral bands shown in Fig. 1 are defined by the manufacturer and correspond to publicly available specifications of the cameras intended for agronomic applications [20]. It is important to note that no modifications were made to the filters or internal construction of the cameras in this study. Consequently, the proposed method can be reproduced using other identical devices.

As the selected cameras were originally intended for long-range imaging, including vegetation acquisition from aerial platforms, their minimum focusing distance is relatively large. Consequently, repurposing them for an intraoperative context requires optical adaptation. Given the characteristics of the original optics, with a minimum focusing distance of approximately 455 cm, and the target working distance of 10-40 cm, macro close-up lenses were applied to shift the focal plane to the required range without disassembling the camera or modifying the existing lens assembly (Fig. 2). This approach enables the depth of focus to be moved closer to the optical centre of the camera, ensuring optimal sharpness within the imaging field and, consequently, technically valid image acquisition.

Both cameras employ glass optics with very low distortion ($\approx -1\%$). The horizontal field of view is approximately 41°, and the focal length (35 mm equivalent) is 47 mm. Still images are recorded at a resolution of 12 MP (4000 × 3000 px) in RAW + JPG formats (12-bit/8-bit), while video is recorded in MP4 (H.264) format at a resolution of 3840 × 2160, with frame rates of 2160p24, 1440p30, 1080p60, and 720p60.

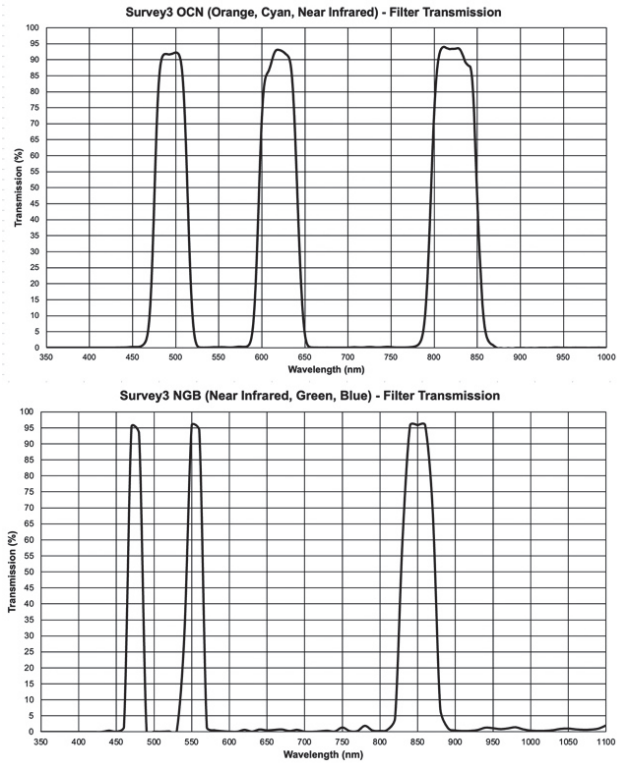

Figure 1 Spectral transmission of the cameras

Issues related to glare and specular reflections in the operating room are well known in standard surgical photography, as moist tissues and metallic instruments produce pronounced reflections. To reduce these effects, circular polarising filters were installed, with their orientation adjusted to the dominant sources of glare within the surgical field. As standard surgical lighting with multiple light sources was used in this study, polarisation filtering enabled the reduction of a substantial portion, though not all, of the reflections. Nevertheless, the most intense reflections that obscured image details were effectively suppressed.

Image acquisition was performed in the operating room in coordination with medical staff and in compliance with sterile protocols, including equipment disinfection, protective clothing, and restricted movement along the periphery of the surgical field. Working distances were maintained within a range of 10-40 cm, with framing adjusted to minimise occlusion of the operative area by the surgical team or instruments. Photographs and short video sequences were captured using the highest resolutions and formats supported by the cameras. For the purposes of this study, still images were selected for analysis, as they enable precise channel separation and storage in 16-bit formats. In addition, still photography allows for greater image magnification and provides higher overall image sharpness compared to video recordings.

Image processing was performed using the Fiji/ImageJ software by applying the Split Channels function to separate composite images into individual spectral channels. The extracted channels were individually evaluated with respect to technical validity, including exposure, sharpness, and morphological readability. The processed images were saved in TIFF format to preserve image quality and to enable consistent comparative analysis.

Figure 2 Camera modification diagram

3 RESULTS

Composite images shown in Fig. 3 revealed information that was not pronounced in standard RGB recordings. However, for more detailed analysis, it was necessary to decompose the images into individual channels in order to examine the contribution of each spectral band separately. Following channel separation, grayscale images were obtained that represent the actual visual intensity values of each spectrally isolated band independently.

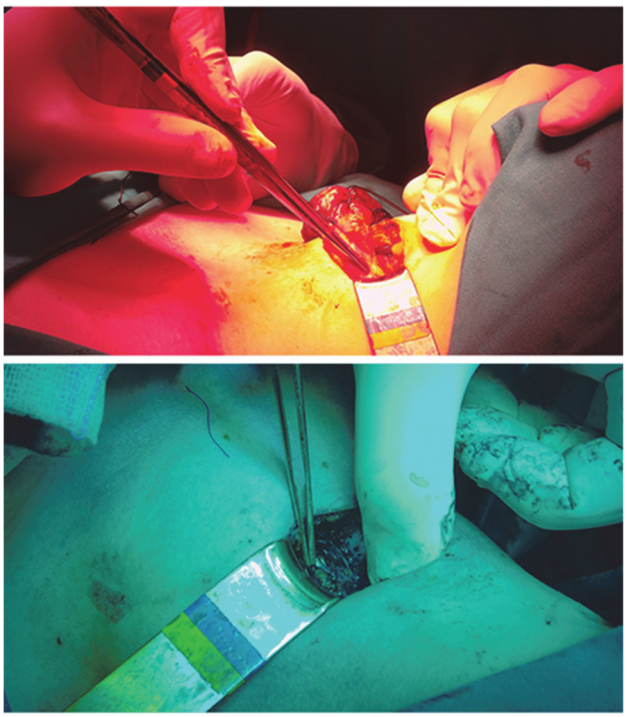

Figure 3 Composite images form the OCN (top) and NGB (bottom) cameras

Images acquired in the orange spectral band at 615 nm (Camera 1, OCN) were technically unsuitable due to overexposure and were therefore excluded from further analysis. Recordings in the cyan spectral band with a peak at 490 nm were technically valid and provided sharp

visualisation of the operative field. The contrast between adipose tissue and thyroid tissue was clearly expressed, facilitating visual differentiation of glandular tissue boundaries (Fig. 4 - top).

The near-infrared band at 808 nm (Camera 1, OCN) consistently emphasised traces of blood and vascular patterns that were less visible or completely obscured in the visible spectrum, even after mechanical cleaning of the operative field, as shown in Fig. 4 (bottom). Compared to visible channels, NIR images at 808 nm systematically revealed information not available in standard RGB systems, which is consistent with previous findings on the utility of NIR imaging for medical visualisation of soft tissues [9, 18].

Figure 4 CYAN 490 nm (top); NIR 808 nm (bottom)

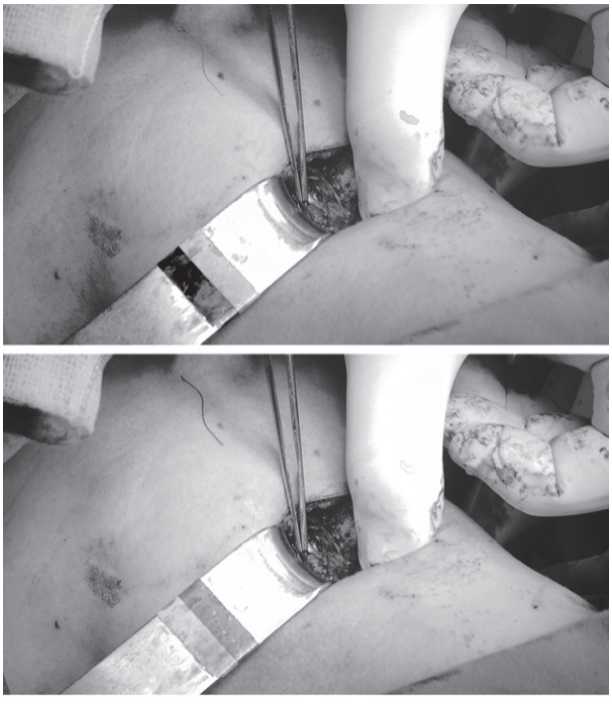

Figure 5 GREEN 550 nm (top); BLUE 475 nm (bottom)

In Camera 2 (NGB), the green channel at 550 nm produced high contrast and clear reproduction of morphological details. As shown in Fig. 5, dark-coloured elements, such as black surgical sutures, are rendered in characteristic grey tones that differ from those observed in other channels. This behaviour further supports the utility of the 550 nm band for visual differentiation of materials and tissues.

Images acquired in the blue spectral band with a peak at 475 nm (Camera 2, NGB) exhibited pronounced surface contrast and accurate reproduction of fine details, which is consistent with the behaviour of shorter wavelengths that emphasise surface structures [9, 12]. Imaging at 850 nm (Camera 2, NGB) was, in this case, entirely unsuitable due to severe underexposure, resulting from insufficient near-infrared illumination in the operating room.

3.1 Quantitative Assessment of Image Quality

A quantitative image quality assessment was performed on 100 × 100 pixel regions of interest (ROIs) across six spectral channels (BLUE 475 nm, CYAN 490 nm, GREEN 550 nm, ORANGE 615 nm, NIR 808 nm, and NIR 850 nm). The analysis included mean gray-level intensity, standard deviation, signal-to-noise ratio (SNR), contrast-to-noise ratio relative to background (CNR), and saturation rates at the maximum (255) and minimum (0) intensity levels.

The SNR was calculated for each ROI as the ratio between the mean gray-level intensity of the ROI (μ_{ROI}) and its corresponding standard deviation (σ_{ROI}), according to:

$$\mathrm{SNR} = \frac{\mu_{\mathrm{ROI}}}{\sigma_{\mathrm{ROI}}} \tag{1}$$

The CNR was calculated relative to the background ROI (BG) as the absolute difference between the mean intensity of the target ROI and the mean intensity of the background, normalized by the standard deviation of the background, according to:

$$\mathrm{CNR} = \frac{\left|\mu_{\mathrm{ROI}} - \mu_{\mathrm{BG}}\right|}{\sigma_{\mathrm{BG}}} \tag{2}$$

These formulations quantify, respectively, the stability of the signal within a given region and the separability of the ROI from the background in the presence of noise. The results are shown in the tables below (Tab. 1 and Tab. 2)

The visible spectral channels (BLUE, GREEN, and CYAN) exhibited a stable and radiometrically balanced response. Mean intensity values within the thyroid ROI were positioned well within the effective dynamic range of the sensor, accompanied by moderate standard deviations, resulting in SNR values on the order of approximately 2.5-3.5., as shown in Fig. 6 and Fig. 7).

In skin and glove ROIs, substantially higher SNR values were consistently observed, indicating homogeneous reflectance and low noise levels. Concurrently, CNR values relative to the background were high across all visible channels, confirming reliable contrast separation between anatomical structures and

surrounding materials. Saturation rates at both 255 and 0 were negligible or very low at the ROI and whole-image levels, indicating preservation of dynamic range and minimal information loss due to clipping.

The ORANGE channel (615 nm) demonstrated extremely high signal intensities and very low intra-ROI variability, leading to exceptionally high SNR and CNR values. However, these numerical indicators coincided with extensive saturation at the maximum intensity level, affecting the majority of pixels within the thyroid, skin, and glove ROIs, as well as a substantial fraction of the entire image. This saturation pattern reflects severe overexposure, whereby the apparent quantitative superiority of the channel is largely artificial and accompanied by a significant loss of grayscale information.

Table 1 OCN camera quantative assesment

ROI (100 × 100)	Mean	StdDev	Min	Max	SNR	CNR (ROI vs BG)	Saturation rate (255) / %	Sat. rate (0) / %
ORANGE (615 nm)								
THY (2130.1140)	252.188	8.200	167	255	30.755	98.073	77.03%	0.00%
SKIN (1240.1460)	254.596	2.330	191	255	109.269	99.154	90.66%	0.00%
GLOVE (3260.430)	254.967	0.933	207	255	273.277	99.320	99.72%	0.00%
BCG (2390.340)	33.681	2.228	28	45	-	-	0.00%	0.00%
SNR control (3250.430)	254.967	0.933	207	255	273.277	-	99.72%	0.00%
Whole image	-	-	-	-	-	-	26.542%	0.00%
CYAN (490 nm)								
THY (2130.1140)	130.057	50.531	0	255	2.574	94.949	0.07%	48.63%
SKIN (1240.1460)	212.004	12.633	89	255	16.782	163.068	0.01%	0.00%
GLOVE (3260.430)	177.083	8.146	123	193	21.739	134.040	0.00%	0.00%
BCG (2390.340)	15.833	1.203	10	21	-	-	0.00%	0.00%
SNR control (3250.430)	179.674	7.049	123	195	25.489	-	0.00%	0.00%
Whole image	-	-	-	-	-	-	020%	5.81%
NIR (808 nm)								
THY (2130.1140)	77.779	33.706	0	230	2.308	51.234	0.00%	3.26%
SKIN (1240.1460)	129.056	13.555	23	183	9.521	93.647	0.00%	0.00%
GLOVE (3260.430)	106.510	3.749	50	120	28.410	74.998	0.00%	0.00%
BCG (2390.340)	15.837	1.209	10	21	-	-	0.00%	0.00%
SNR control (3250.430)	107.337	3.708	50	120	28.947	-	0.00%	0.00%
Whole image	-	-	-	-	-	-	0.35%	0.68%

Table 2 NGB camera quantative assesment

ROI (100 × 100)	Mean	StdDev	Min	Max	SNR	CNR (ROI vs BG)	Saturation rate (255) / %	Sat. rate (0) / %
NIR (850 nm)								
THY (1930.1280)	4.590	9.376	0	111	0.490	1.925	0.00%	55.15%
SKIN (1300.900)	0.000	0.000	0	0	0.000	1.532	0.00%	100.00%
GLOVE (3560.660)	0.000	0.000	0	0	0.000	1.532	0.00%	18.05%
BCG (2820.790)	2.034	1.328	0	6	1.532	-	0.00%	100.00%
SNR control (3660.790)	0.000	0.000	0	0	0.000	-	0.00%	100.00%
Whole image	-	-	-	-	-	-	0.008%	86.46%
GREEN (550 nm)								
THY (1930.1280)	89.061	31.672	23	207	2.812	26.969	0.00%	0.00%
SKIN (1300.900)	203.859	3.669	194	215	55.563	74.544	0.00%	0.00%
GLOVE (3560.660)	201.402	4.032	179	210	49.951	73.526	0.00%	0.00%
BCG (2820.790)	23.984	2.413	18	31	9.939	-	0.00%	0.00%
SNR control (3660.790)	184.458	5.514	169	199	33.453	-	0.00%	0.00%
Whole image	-	-	-	-	-	-	2.433%	0.00%
BLUE (475 nm)								
THY (1930.1280)	81.102	23.320	27	201	3.478	28.850	0.00%	0.00%
SKIN (1300.900)	184.536	3.362	176	197	54.889	83.577	0.00%	0.00%
GLOVE (3560.660)	187.946	3.049	175	195	61.642	85.381	0.00%	0.00%
BCG (2820.790)	26.575	1.890	21	34	14.061	-	0.00%	0.00%
SNR control (3660.790)	172.404	5.842	156	186	29.511	-	0.00%	0.00%
Whole image	-	-	-	-	-	-	0.877%	0.29%

The near-infrared channels exhibited wavelength-dependent behavior. The NIR channel at 808 nm showed a moderately balanced radiometric response, with limited but usable SNR values in the thyroid ROI and higher SNR and CNR values in skin and glove regions. Saturation at both intensity extremes was minimal, indicating a preserved dynamic range and appropriate exposure conditions. In contrast, the NIR channel at 850 nm was characterized by extremely low mean signal levels, relatively high noise, and very low SNR values in the thyroid ROI. The dominant saturation at the minimum intensity level across ROIs and the entire image clearly indicates pronounced underexposure and insufficient sensor sensitivity at this wavelength.

Whole-image saturation analysis further corroborated these trends. Visible BLUE, GREEN and CYAN channels, as well as NIR 808 nm maintained low fractions of saturated pixels, the ORANGE channel exhibited dominant saturation at the upper intensity limit, and the NIR 850 nm channel showed widespread saturation at the lower intensity limit. These patterns directly reflect differences in spectral sensor response.

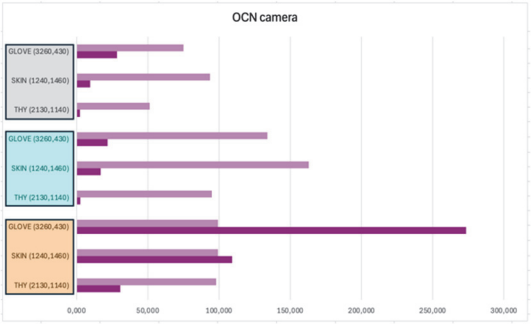

Figure 6 OCN camera results

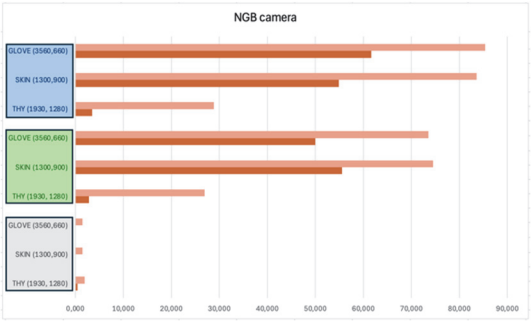

Figure 7 NGB camera results

These quantitative findings are consistent with the visual inspection of the multispectral images, where channels exhibiting moderate SNR, high CNR, and low saturation rates provide clear and stable visual differentiation between the thyroid, surrounding tissues, and background. Conversely, channels affected by extensive saturation or underexposure show reduced visual contrast and loss of structural detail, confirming that the quantitative metrics reliably reflect the perceived image quality and practical interpretability of the images.

4 CONCLUSION

This study demonstrates that agronomic multispectral cameras, originally intended for aerial imaging applications, can be successfully adapted for photographic documentation of human tissue under intraoperative conditions in endocrine surgery. Optical adaptation of the minimum focusing distance using macro close-up lenses enabled stable imaging of the target area at working distances of 10-40 cm while preserving the low distortion characteristics of the optical system. The application of polarising filters effectively reduced specular reflections within the surgical field, and spectral channel separation combined with TIFF export ensured reproducibility and comparability of recordings between cameras. All adaptations were implemented without disrupting surgical workflow and in compliance with sterile procedures, thereby confirming the operational feasibility and repeatability of the proposed modifications and results under real clinical conditions.

The results of multispectral imaging indicate that a limited set of selected wavelengths can provide stable and additional information on soft tissues of the neck and thyroid gland, without the use of contrast agents and without interference with the surgical workflow. The 490 nm channel consistently enhanced contrast between adipose tissue and thyroid parenchyma, while the 550 nm channel demonstrated high informational value in the region of the parathyroid glands. The differing reproduction of certain artificial materials in the 550 nm and 475 nm channels further highlights the potential of the visible spectrum for differentiating materials and tissues within the surgical field. The near-infrared channel at 808 nm revealed information that was weakly visible or not visible in the visual spectrum, implying that reflectance-based NIR imaging can support the identification of relevant anatomical structures without the use of specialised medical equipment.

At the same time, clear technical limitations of the existing configuration were identified. Images acquired in the orange spectral band at 615 nm (Camera 1, OCN) were found to be technically unsuitable due to systematic overexposure and were therefore not appropriate for further analysis. This outcome indicates higher sensitivity of the orange channel compared to the cyan and NIR channels, which in future acquisitions will require compensation through increased illumination in the NIR and cyan spectral ranges. Imaging at 850 nm (Camera 2, NGB) was, in this study, entirely unusable due to pronounced underexposure caused by the lack of an infrared component in the existing surgical lighting. As a result, no usable information was obtained in this channel, clearly indicating the need to introduce an additional NIR light source in future studies in order to achieve the full potential of imaging at 850 nm.

In a pedagogical context, the multispectral layer can complement existing 2D and 3D recordings and support perception-based learning derived from photographic and video materials in medical education. This form of multispectral camera repurposing represents an enhanced approach to recording information that is not visible to the unaided eye, with reproduction suitable for subsequent use in educational and research environments.

The proposed technical adaptations enable reliable and reproducible production of multispectral photographic material that is sufficiently informative for the visual differentiation of structures relevant to endocrine surgery.

This study is conceived as a preliminary investigation, intended to establish the technical feasibility and methodological framework of the proposed approach, with clear potential for further development, optimization, and validation in larger and more diverse clinical datasets.

5 REFERENCES

[1] Ancic, M., Pernar, R., Bajic, M., Krtalic, A., Seletkovic, A., Gajski, D., & Kolic, J. (2020). Spectral signatures (Endmembers) some of forest species in the republic of Croatia. *Sumarski List*, *144*(3-4), 119-127. https://doi.org/10.31298/sl.144.3-4.1

[2] Ma, F., Yuan, M., & Kozak, I. (2023). Multispectral imaging: Review of current applications. *Survey of Ophthalmology*, *68*(5), 889-904. https://doi.org/10.1016/j.survophthal.2023.06.004

[3] Berger, K., Machwitz, M., Kycko, M., Kefauver, S. C., Van Wittenberghe, S., Gerhards, M., Verrelst, J., Atzberger, C., et al. (2022). Multi-sensor spectral synergies for crop stress detection and monitoring in the optical domain: A review. Remote sensing of environment, *280*, 113198. https://doi.org/10.1016/j.rse.2022.113198

[4] Dunker, S., Boyd, M., Durka, W., Erler, S., Harpole, W. S., Henning, S., Herzschuh, U., Hornick, T., Knight, T., Lips, S.,

Mäder, P., Švara, E. M. et al. (2022). The potential of multispectral imaging flow cytometry for environmental monitoring. *Cytometry, Part A : the journal of the International Society for Analytical Cytology*, *101*(9), 782-799. https://doi.org/10.1002/cyto.a.24658

[5] Spreinat, A., Selvaggio, G., Erpenbeck, L., & Kruss, S. (2020). Multispectral near infrared absorption imaging for histology of skin cancer. *Journal of Biophotonics*, *13*(1), e201960080. https://doi.org/10.1002/jbio.201960080

[6] Corda, D. N. & Grsic, J. Z. (2021). Extended method of restoration retouching in the near-infrared spectrum. *8th SWS International Scientific Conferences on SOCIALSCIENCES - ISCSS Proceedings 2021*, *8*, 571-584. https://doi.org/10.35603/sws.iscss.va2021/s10.65

[7] Paras, C., Keller, M., White, L., Phay, J., & Mahadevan-Jansen, A. (2011). Near-infrared autofluorescence for the detection of parathyroid glands. *Journal of Biomedical Optics*, *16*(6), 067012. https://doi.org/10.1117/1.3583571

[8] Demarchi, M. S., Karenovics, W., Bédat, B., & Triponez, F. (2021). Near-infrared fluorescent imaging techniques for the detection and preservation of parathyroid glands during endocrine surgery. *Innovative surgical sciences*, *7*(3-4), 87-98. https://doi.org/10.1515/iss-2021-0001

[9] Barberio, M., Maktabi, M., Gockel, I., Rayes, N., Jansen-Winkeln, B., Köhler, H., Rabe, S. M., Seidemann, L., Takoh, J. P., Diana, M., Neumuth, T., & Chalopin, C. (2018). Hyperspectral based discrimination of thyroid and parathyroid during surgery: Hyperspectral imaging for tissue discrimination. *Current Directions in Biomedical Engineering*, *4*(1), 399-402. https://doi.org/10.1515/cdbme-2018-0095

[10] Solórzano, C. C., Thomas, G., Berber, E., Wang, T. S., Randolph, G. W., Duh, Q. Y., & Triponez, F. (2021). Current state of intra operative use of near infrared fluorescence for parathyroid identification and preservation. *Surgery*, *169*(4), 868-878. https://doi.org/10.1016/j.surg.2020.09.014

[11] Wang, B., Zhu, C. R., Liu, H., Yao, X. M., & Wu, J. (2021). The accuracy of near infrared autofluorescence in identifying parathyroid gland during thyroid and parathyroid surgery: A meta-analysis. *Frontiers in Endocrinology*, *12*, 701253. https://doi.org/10.3389/fendo.2021.701253

[12] Maktabi, M., Köhler, H., Ivanova, M., Neumuth, T., Rayes, N., Seidemann, L., Sucher, R., Jansen-Winkeln, B., Gockel, I., Barberio, M., & Chalopin, C. (2020). Classification of hyperspectral endocrine tissue images using support vector machines. *International Journal of Medical Robotics and Computer Assisted Surgery*, *16*(5), 1-10. https://doi.org/10.1002/rcs.2121

[13] Setchfield, K., Gorman, A., Simpson, A. H. R. W., Somekh, M. G., & Wright, A. J. (2023). Relevance and utility of the in-vivo and ex-vivo optical properties of the skin reported in the literature: A review [Invited]. *Biomedical Optics Express*, *14*(7), 3555-3583. https://doi.org/10.1364/BOE.493588

[14] Colas, V., Blondel, W., Khairallah, G., Daul, C., & Amouroux, M. (2021). Proposal for a skin layer-wise decomposition model of spatially-resolved diffuse reflectance spectra based on maximum depth photon distributions: A numerical study. *Photonics*, *8*(10), 444. https://doi.org/10.3390/photonics8100444

[15] Serrage, H., Heiskanen, V., Palin, W. M., Cooper, P. R., Milward, M. R., Hadis, M., & Hamblin, M. R. (2019). Under the spotlight: mechanisms of photobiomodulation concentrating on blue and green light. *Photochemical & Photobiological Sciences*, *18*(8), 1877-1909. https://doi.org/10.1039/c9pp00089e

[16] Jiang, Z., Gu, X., Chen, D., Zhang, M., & Xu, C. (2024). Deep learning-assisted multispectral imaging for early screening of skin diseases. *Photodiagnosis and Photodynamic Therapy*, *48*, 104292. https://doi.org/10.1016/j.pdpdt.2024.104292

[17] Ilișanu, M. A., Moldoveanu, F., & Moldoveanu, A. (2023). Multispectral Imaging for Skin Diseases Assessment-State of the Art and Perspectives. *Sensors*, *23*(8), 3888. https://doi.org/10.3390/s23083888

[18] Rey-Barroso, L., Burgos-Fernández, F. J., Delpueyo, X., Ares, M., Royo, S., Malvehy, J., Puig, S., & Vilaseca, M. (2018). Visible and extended Near-infrared multispectral imaging for skin cancer diagnosis. *Sensors*, *18*(5), 1441. https://doi.org/10.3390/s18051441

[19] Kulawardhana, R. W. (2011). Remote sensing of vegetation: principles, techniques and applications. *Journal of Vegetation Science*, *22*(6), 1151-1153. https://doi.org/10.1111/j.1654-1103.2011.01319.x

[20] See https://www.mapir.camera/pages/survey3-cameras

[21] Yaow, C. Y. L., Mok, H. T., Ng, C. H., Devi, M. K., Iyer, S., & Chong, C. S. (2020). Difficulties Faced by General Surgery Residents. A Qualitative Systematic Review. *Journal of Surgical Education*, *77*(6), 1396-1406. https://doi.org/10.1016/j.jsurg.2020.06.003

[22] Grsic, K., Malic, M., & Bilos, J. (2021). 2D and 3D Video of thyroid surgery-right thyroid lobectomy (with Video). *European Annals of Otorhinolaryngology, Head and Neck Diseases*, *138*, 39-40. https://doi.org/10.1016/j.anorl.2021.03.012

[23] Rajković, I., Radonić, D., Grsic, K., & Žiljak Gršić, J. (2020). 3d Video as a practice-learning module in surgical education. *EDULEARN20 Proceedings*, 2871-2876. https://doi.org/10.21125/edulearn.2020.0862

[24] Hoyek, N., Collet, C., Di Rienzo, F., De Almeida, M., & Guillot, A. (2014). Effectiveness of three-dimensional digital animation in teaching human anatomy in an authentic classroom context. *Anatomical Sciences Education*, *7*(6), 430-437. https://doi.org/10.1002/ase.1446

[25] Guo, J., Guo, Q., Feng, M., Liu, S., Li, W., Chen, Y., & Zou, J. (2023). The use of 3D video in medical education: A scoping review. *International Journal of Nursing Sciences*, *10*(3), 414-421. https://doi.org/10.1016/j.ijnss.2023.06.006

[26] Ahmet, A., Gamze, K., Rustem, M., & Karaborklu Argut, S. (2018). Is Video-Based Education an Effective Method in Surgical Education? A Systematic Review. *Journal of Surgical Education*, *75*(5), 1150-1158. https://doi.org/10.1016/j.jsurg.2018.01.014

[27] Bordes, S. J., Walker, D., Modica, L. J., Buckland, J., & Sobering, A. K. (2021). Towards the optimal use of video recordings to support the flipped classroom in medical school basic sciences education. *Medical Education Online*, *26*(1), 1841406. https://doi.org/10.1080/10872981.2020.1841406

Contact information:

Dinka RADONIĆ
(Corresponding author)
Zagreb University of Applied Sciences,
Vrbik 8, 10000 Zagreb, Croatia
E-mail: dinka.radonic@tvz.hr

Jana ŽILJAK GRŠIĆ
Zagreb University of Applied Sciences,
Vrbik 8, 10000 Zagreb, Croatia
E-mail: jana@tvz.hr

Ivan RAJKOVIĆ
Zagreb University of Applied Sciences,
Vrbik 8, 10000 Zagreb, Croatia
E-mail: ivan.rajkovic@tvz.hr

Krešimir GRŠIĆ
University Hospital Centre Zagreb,
Ulica Mije Kišpatića 12, 10000, Zagreb, Croatia
E-mail: kresimir.grsic@gmail.com